



---

# Phononics

---

2015

3<sup>rd</sup> INTERNATIONAL CONFERENCE ON PHONONIC CRYSTALS/  
METAMATERIALS, PHONON TRANSPORT & PHONON COUPLING

May 31-June 5, 2015 – Paris, France



## *2015 Brillouin Medal Recipients:*

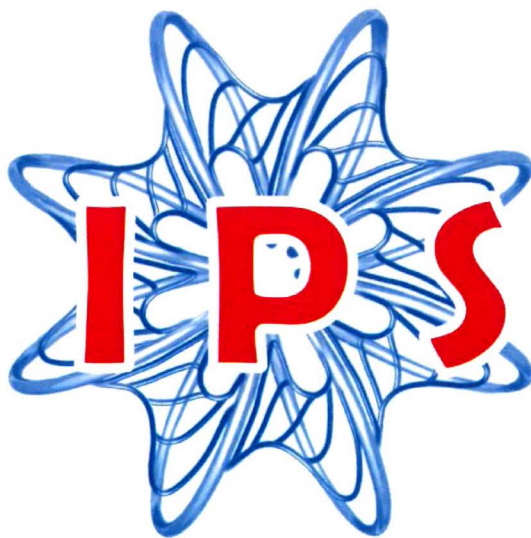
*John H. Page*

*Department of Physics and Astronomy  
University of Manitoba, Canada*

*Zhengyou Liu*

*School of Physics and Technology  
Wuhan University, China*

*Suxia Yang*



INTERNATIONAL PHONONICS SOCIETY

## Focusing of acoustic waves by negative refraction in phononic crystals.

John H. Page<sup>1</sup>, Zhengyou Liu<sup>2</sup> and Suxia Yang<sup>3</sup>

<sup>1</sup> *Department of Physics and Astronomy, University of Manitoba, Winnipeg, Manitoba, Canada R3T 2N2*

<sup>2</sup> *Department of Physics, Wuhan University, China*

<sup>3</sup> *Xerox Research Centre of Canada, 2660 Speakman Drive, Mississauga, Ontario, Canada L5K 2L1*

**Abstract:** We review negative refraction and focusing phenomena in phononic crystals, from their initial discovery more than 10 years ago in flat three-dimensional (3D) phononic crystals to more recent work demonstrating how super-resolution focusing can be achieved. Ultrasonic experiments, in combination with theory and simulations, have played an important role in developing a detailed understanding of these phenomena.

### 1. Introduction

The focusing of phonons and acoustic waves in crystals has a long history that predates the recent interest in phononic crystals. The phenomenon called “phonon focusing” started with observations that heat flux in the low temperature ballistic transport regime of atomic crystals is channeled along particular directions due to elastic anisotropy<sup>1</sup>. Since this phonon focusing effect is observed at long wavelengths compared with the lattice constants of atomic crystals, continuum elasticity can be used to explain the experiments. Phonon focusing occurs because in elastically anisotropic media, the group velocity  $\mathbf{v}_g$  and wavevector  $\mathbf{k}$  are not parallel in general, with the result that waves with different  $\mathbf{k}$  can have similar  $\mathbf{v}_g$ , and the energy flux, which follows the direction of the group velocity, is therefore channeled along certain crystalline directions. This focusing effect has been observed in a wide variety of experiments, from heat pulse transport to ultrasonic propagation from a point-like source, with the experimental evidence and physical interpretation being comprehensively reviewed in the book by J.P. Wolfe<sup>2</sup>.

During the explosion of activity in phononic crystal research at the end of the 1990s and early 2000s, it therefore seemed natural to us to ask whether interesting and possibly different focusing and imaging phenomena could occur in phononic crystals. About this time, it became widely recognized that doubly negative materials, with simultaneously negative electric permittivity and magnetic permeability for electromagnetic waves, or with negative modulus and mass density for acoustic waves, have a negative refractive index, with the Poynting vector ( $\propto \mathbf{v}_g$ ) and  $\mathbf{k}$  pointing in opposite directions. At the interface between positive and doubly negative materials, waves are therefore refracted negatively, which is the basis of Pendry’s “perfect lens”<sup>3</sup>. We were curious to see if focusing by negative refraction could also be observed in phononic crystals, in this case due to the effects of Bragg scattering on the crystal’s band structure, which might cause  $\mathbf{v}_g$  and  $\mathbf{k}$  to be of opposite sign.

In this paper, we review the research on negative refraction and focusing in phononic crystals that has been initiated by ultrasonic experiments performed at the University of Manitoba. These experiments capitalized on our ability to construct high quality 3D and 2D phononic crystals and to use the versatility of ultrasonic techniques to measure phononic crystal properties with excellent resolution in space, time and frequency. We begin with our early work on focusing in a 3D phononic crystal<sup>4</sup>, and then summarize more recent work on negative refraction<sup>5</sup> and super-resolution focusing in 2D crystals<sup>6</sup>.

### 2. Focusing of ultrasound in a 3D phononic crystal

Our experiments on a three-dimensional phononic crystal consisting of 0.800-mm-diameter tungsten-carbide beads immersed in water were the first to demonstrate ultrasound focusing by negative refraction<sup>4</sup>, initiating a new direction in phononic crystal research that has been very active over the last decade<sup>7,8</sup>, and continues to attract considerable attention, especially now for acoustic metamaterials. The beads were close packed in the face-centred-cubic structure, and the crystal consisted of a 12-layer-thick slab with the [111] direction perpendicular the layers. In this crystal, focusing effects were discovered at frequencies in the pass band near 1.6 MHz, which is above the complete band gap that occurs between 0.98 and 1.2 MHz<sup>9</sup> and is therefore in a frequency range where behaviour most analogous to negative refraction focusing in doubly negative materials could occur. In our experiments, a small source consisting of a pinducer (radius  $\sim \lambda$ , where  $\lambda$  is the wavelength in water) was placed close to the sample surface (3 mm, or approximately  $2\lambda$  away), and the field pattern on the far side of the crystal and its substrate was measured by scanning a small hydrophone (diameter  $\ll \lambda$ ) in a plane parallel to the crystal surface - see Fig. 1(a). The experiments were performed with pulses. By taking the Fourier transforms of each transmitted pulse,

the amplitude of the transmitted field at any frequency in the bandwidth of the pulse could then be measured as a function of position in the detecting plane. As the frequency was varied, the detected field pattern varied widely, a result of rapid changes in the anisotropy of the dispersion relations with frequency. Figure 1(b) shows the measured field pattern at 1.57 MHz. At this frequency, the diverging beam from the pinducer, which has a FWHM in the detection plane of 65 mm (more than three quarters of the width of the region imaged in the figure), was sharply focused to a tight spot with a FWHM of only 5 mm. This example showed clearly that a phononic crystal with flat parallel planar faces can be used to focus ultrasound. One remarkable feature of these data is that such a sharp focal spot is observed in a plane quite far from the crystal; the distance from the crystal face to the detection plane is approximately 130 wavelengths, while the distance from the source to the crystal is only 2 wavelengths.

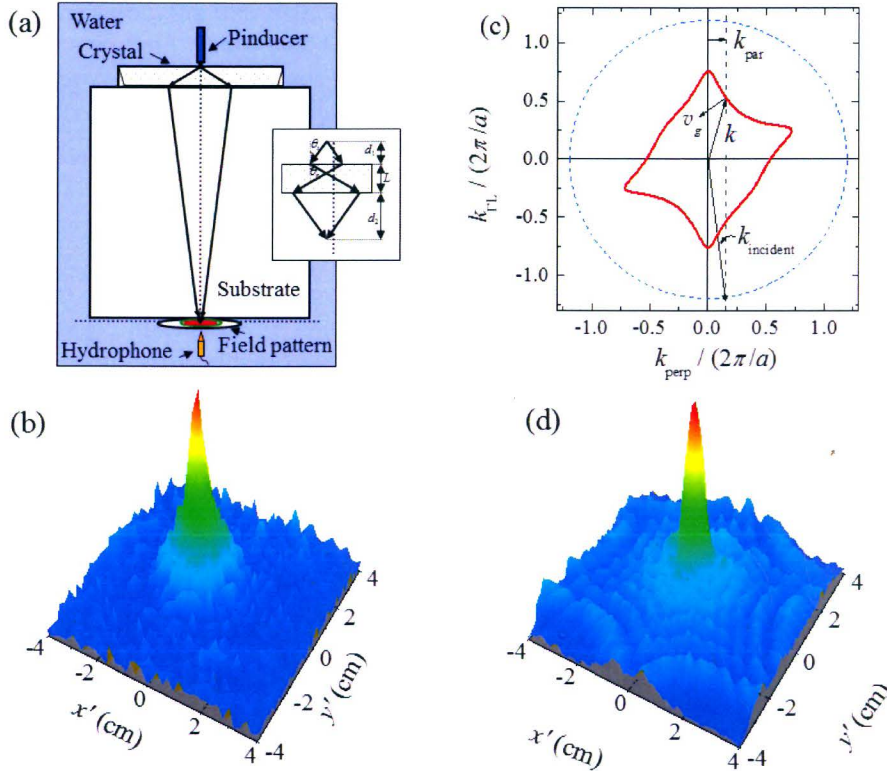


**Figure 1** (a) Schematic representation of the experimental setup, with the arrows between the source and detector indicating the direction of the group velocity. The inset shows the focusing condition for a negative index medium. (b) Image of the source focused by a 12-layer phononic crystal made from tungsten carbide beads.

(c) Cross section of the equifrequency surfaces of this phononic crystal at 1.57 MHz in a plane containing the [111], [110] and [001] directions. The dashed circle is the equifrequency contour for water. (d) Calculated field pattern using a Fourier imaging technique, based on the 3D equifrequency surface predicted by the MST. Adapted from Ref. 4.

The origin of the focusing effect was understood by examining the equifrequency surfaces, which represent the variation in the magnitude of the wave vector with direction at a given frequency. Figure 1(c) shows a cross section in a plane containing the [111] direction of the 3D equifrequency surface at 1.57 MHz, calculated in the reduced zone scheme using the Multiple Scattering Theory (MST)<sup>10</sup>. Also shown by the dashed curve is the equifrequency surface for water, and a representative incident wave vector  $\mathbf{k}_{\text{incident}}$  inclined away from the normal to the surface of the crystal. The directions of  $\mathbf{k}$  and  $\mathbf{v}_g$  for the corresponding Bloch waves inside the crystal are also shown; these directions are determined by the boundary conditions that the component of the wave vector parallel to the surface ( $k_{\text{par}} \perp k_{\text{TL}}$ ) must be equal both inside and outside the crystal (Snell's law) and the condition that  $\mathbf{v}_g$  is normal to the equifrequency surface, since  $\mathbf{v}_g = \nabla_{\mathbf{k}} \omega(\mathbf{k})$ . For the waves to travel through the crystal, the group velocity must have a component pointing towards the opposite side of the crystal, and this can only be achieved if  $\mathbf{v}_g$  points in a direction that corresponds to a negative angle of refraction. This occurs even though the wave vector obeys Snell's law in the usual way at each interface. It is this large negative refraction of Bloch waves inside the crystal, governed by the directions of the group velocity, that allows an image of the source to be formed on the far side of the crystal and substrate, as shown schematically by the "rays" drawn in Fig. 1(a).

To further elucidate the imaging mechanism, the shape of the image was calculated using a Fourier imaging technique, in which the input beam was Fourier transformed spatially into plane waves, with each plane wave propagating through the crystal according to the wave vectors determined by the equifrequency surface. The boundary conditions at the front and back interfaces were correctly

implemented according to Snell's law. The image in the detecting plane was then reconstructed by taking an inverse Fourier transform back into real space, giving the results shown in Fig. 1(d). Excellent agreement with experiment is seen, confirming that this model correctly incorporates the essential physics of this wave-focusing phenomenon. Thus we were able to determine directly the focusing mechanism and to show how this mechanism can be simply described in terms of negative refraction. We emphasize that, despite the similarities with negative refraction in doubly negative metamaterials<sup>3</sup>, where negative refraction arises from local resonances, the origin of negative refraction in phononic crystals is a band-structure effect; in both cases, the direction of energy transport due to negative refraction is determined by Poynting's vector, and for phononic crystals it is always given by the direction of the group velocity<sup>4</sup>.

### 3. Direct observation of negative refraction in phononic crystals

To explore the phenomena of negative refraction in phononic crystals in more detail, a number of experiments and theoretical calculations have been performed on 2D crystals<sup>5, 11-13</sup>. The most direct observations of negative refraction were made by Sukhovich *et al.*<sup>5</sup>, who constructed a prism-shaped phononic crystal of steel rods, arranged in a triangular lattice at a volume fraction of 58% and surrounded by water. This crystal has the advantage of a relatively simple band structure, as shown by the solid curves (MST) and symbols (experiment) in Fig. 2(a). The second pass band, between the stop band along  $\Gamma M$  and the band gap near 1 MHz, has a single branch,

which appears isotropic. This isotropic behaviour is confirmed by the equifrequency contours (Fig. 2(b)). The contours are remarkably circular and shrink in radius as the frequency increases, indicating that the wave vector has the same magnitude in all directions, and that the group velocity  $\mathbf{v}_g$  points towards the centre of each circular contour. Thus, for this band, the group velocity and wave vector in the first Brillouin zone are antiparallel for all directions of propagation, as for left-handed behaviour in negative index metamaterials<sup>3</sup>, and waves arriving at the surface of the crystal at non-normal incidence will be negatively refracted. This effect is demonstrated by the experimental data shown in Fig. 2(c), which was obtained by directing a narrowband pulse with central frequency 0.85 MHz towards the shortest face of the prism at normal incidence (see the wide blue arrow) and imaging the field that emerged from the longest face using a miniature hydrophone. Since the wave pulse enters the crystal at normal incidence, the pulse continues to travel inside the crystal in the original direction, which is parallel to the group velocity. As the pulse leaves the crystal, the outgoing field pattern is seen to bend backwards in the negative direction, showing, according to Snell's law, that the wave vector inside the crystal must also point in the negative direction, opposite to the direction of the group velocity, as predicted from the equifrequency contour. To emphasize this point, the directions of the Bloch wave vector and group velocity inside the crystal are also shown in Fig. 2(c), as well as the

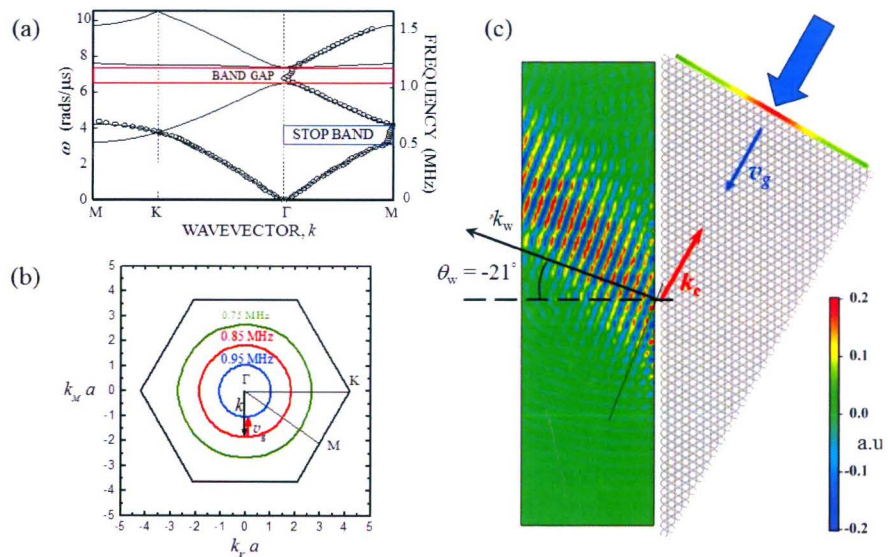


**Figure 2** (a) Band structure of a phononic crystal of steel rods in water (triangular lattice of 1.02-mm-diameter rods with lattice constant  $a = 1.27$  mm). The solid curves were calculated using Multiple Scattering Theory calculations, and the symbols represent experimental data. (b) MST equifrequency contours at the three frequencies, 0.75, 0.85 and 0.95 MHz, in the second pass band. (c) Snapshot the negatively-refracted pulse emerging from a phononic crystal prism (angles  $30^\circ$ ,  $60^\circ$  and  $90^\circ$ , as shown) after a narrow-band pulse (central frequency of 0.85 MHz) was normally incident on the shortest face of the prism (in the direction of wide blue arrow). The data were measured by scanning a hydrophone in a rectangular grid, digitally filtering the pulses to narrow the bandwidth, and measuring the wave field at a particular moment in time to construct the spatial variation of the field at that time. Adapted from Ref. 5.

experimental data shown in Fig. 2(c), which was obtained by directing a narrowband pulse with central frequency 0.85 MHz towards the shortest face of the prism at normal incidence (see the wide blue arrow) and imaging the field that emerged from the longest face using a miniature hydrophone. Since the wave pulse enters the crystal at normal incidence, the pulse continues to travel inside the crystal in the original direction, which is parallel to the group velocity. As the pulse leaves the crystal, the outgoing field pattern is seen to bend backwards in the negative direction, showing, according to Snell's law, that the wave vector inside the crystal must also point in the negative direction, opposite to the direction of the group velocity, as predicted from the equifrequency contour. To emphasize this point, the directions of the Bloch wave vector and group velocity inside the crystal are also shown in Fig. 2(c), as well as the

direction of  $\mathbf{k}$  for the refracted beam outside, which is perpendicular to the wave fronts<sup>a</sup>. Furthermore, the measured refraction angle is given within experimental uncertainty by Snell's law, using the value of the wave vector inside the crystal predicted by MST, providing additional evidence that the data can be quantitatively described in terms of negative refraction.

#### 4. Super-resolution focusing

To investigate the ultimate image resolution that may be possible with a flat lens made from this 2D phononic crystal, a rectangular-shaped six-layer crystal of steel rods with the same crystal structure was constructed<sup>5</sup>. Each layer contained 60 rods (to avoid edge effects), and the layers were stacked in the  $\Gamma M$  direction, *i.e.*, with the base of the triangular unit cell parallel to the surface. The resolution capabilities of the lens were explored using a narrow line source (width 0.55 mm, which is less than the wavelength in water at the frequencies of interest), which was built in the lab from piezoelectric polymer strips. To ensure that the equifrequency contours inside and outside the crystal would be the same size, so that an effective refractive index of -1 could be attained, the crystal was built with thin transparent walls so that the liquid inside the crystal could be methanol, which has a lower sound velocity than water, shrinking the frequency axis of the dispersion curve shown in Fig 2 (a) by 74%. As a result, the equifrequency contours of both the crystal and the water outside were perfectly matched at a frequency of 0.55 MHz in the second band. Thus, all angle negative refraction (AANR) was achieved at this frequency, and all others down to the bottom of the band at 0.50 MHz. The image obtained at 0.55 MHz, when the source was placed 1.6 mm from the opposite surface of the crystal, is shown in Fig. 3(a). A good focal pattern is clearly seen, with the focal spot narrowly confined both perpendicular and parallel to the crystal surface. By fitting a sinc function (Fig. 3(b)), the transverse width of the image was measured to be 3.0 mm, with a corresponding resolution of  $0.55 \lambda$ , as determined by the Rayleigh criterion (resolution equals half the full width of the peak,  $\Delta$ , *i.e.*, the distance from the maximum to the adjacent minimum (zero)). This shows that a flat phononic crystal with equifrequency contours matched to those of the medium outside can produce images with an excellent resolution approaching the diffraction limit of  $\lambda/2$ <sup>5</sup>.

To achieve super resolution (better than the diffraction limit), it is necessary to capture and amplify evanescent waves from the source - something that clearly did not occur for the data shown in Fig. 3(a). However, when the source was brought even closer to the surface of the crystal, 0.1 mm or  $\lambda/25$  away, significantly improved resolution was obtained<sup>6</sup>. The best resolution was found at a slightly lower frequency, 0.53 MHz, as shown by the experimental results in Fig. 3(c), which are compared with Finite Difference Time Domain (FDTD) simulations in Figs. 3(d)-(f). Good agreement between experiment and simulations was found. Both the experimental and theoretical resolutions,  $0.37 \lambda$  and  $0.35 \lambda$ , are clearly better than the diffraction limit. The reason why super resolution can be attained for this very small source-crystal separation is that some of the evanescent waves from the source are now able to couple to a bound mode of the crystal, and hence become amplified sufficiently to participate in image restoration. Evidence for the excitation of this bound mode can be seen in the field patterns of Figs. 3(c) and (e), which show several subsidiary peaks that are largest at the crystal surface; these additional peaks (not seen in (a)) decay rapidly with distance from the crystal, as expected for the evanescent decay of bound crystal modes. Additional evidence for the existence of this bound mode was obtained from FDTD calculations of the band structure of a finite crystal slab with the same number of layers as in the experiment. These calculations revealed a nearly flat band that extends from 0.525 MHz at the water line to 0.51 MHz at the zone boundary; as it lies below the water line, this mode is bound to the crystal slab since it cannot propagate in water. The best focusing is seen at 0.53 MHz, as this frequency lies between the frequency for perfectly matched equifrequency contours (0.55 MHz) and the resonance frequencies of the bound mode (0.51 - 0.525 MHz), but is still close enough to the bound mode that it can be excited. Calculations of the field patterns inside the phononic crystal indicate that this bound mode is a slab mode of the crystal, and not a surface mode.

<sup>a</sup> Note that to measure the direction of  $k$ , it crucial to measure the wave field and not just the intensity so that  $\mathbf{k}$  can be determined from the wave fronts, as the position of maximum intensity in the refracted beam in this pulsed experiment is also influenced by the time the pulse reached the exit surface of the crystal, with the earlier arrivals being closer to the top of the prism and corresponding to the signals on the top left part of the measurement area.

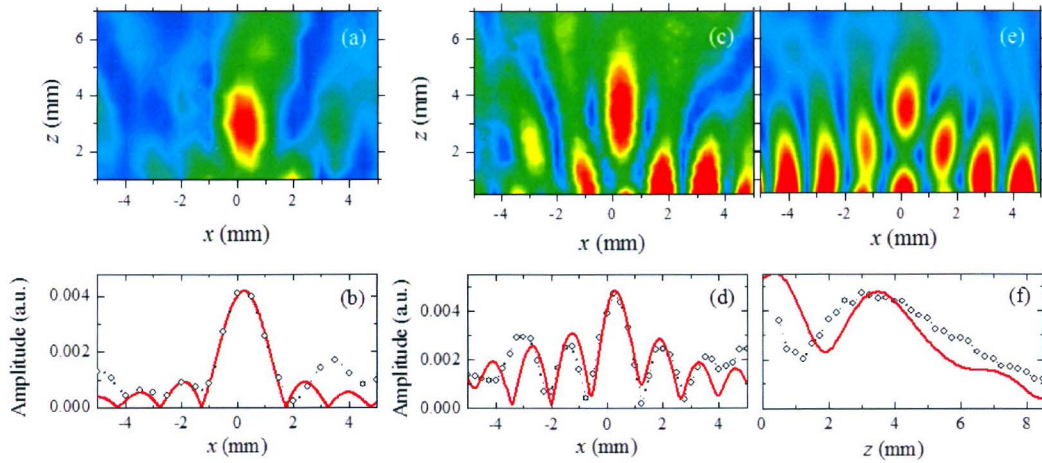


**Figure 3** Contour maps of the ultrasonic amplitude (magnitude of the FFT of the wave field at the frequencies indicated) on the imaging side of a flat methanol-steel phononic crystal lens for a 0.55-mm-wide line source, and corresponding plots of the amplitude through the focus. (a): Image measured at 0.55 MHz for a source-lens distance of 1.6 mm. (b): Amplitude parallel to the lens surface (circles) through the focus in (a). The data are compared with a sinc function (red line), indicating a resolution  $\Delta/2 = 0.55 \lambda$ . (c) and (e): Images measured (c) and calculated with FDTD (e) for a frequency of 0.53 MHz when the source-lens distance is only 0.1 mm. Note the appearance of a bound mode of the crystal, which decays evanescently as the distance from the surface (at  $z = 0$ ) increases. (d) and (f): Comparison of experiment (circles) and simulations (solid curves) for the transverse width of the focal spot (d) and its variation with distance from the surface of the crystal (f). Super resolution is evident from the half widths of the primary peaks in (d), giving a resolution of  $0.37 \lambda$  and  $0.35 \lambda$  for experiment and simulations, respectively. Adapted from Refs. 5 and 6.

This demonstration that super resolution can be achieved in practice with phononic crystal lenses enabled a detailed study of the many factors that can influence the optimum resolution<sup>14</sup>. One of the most interesting questions concerns the mechanism that sets the resolution limit for this crystal. This limit is determined by the largest transverse wave vector  $k_{\max}$  that the crystal will support, which is expected to be the wave vector at the Brillouin zone boundary of the crystal along the  $\Gamma K$  direction (parallel to the surface of the lens)<sup>14, b</sup>. This condition gives  $k_{\max} = 4\pi/3a$ . If we assume perfect transmission for all transverse wave vectors  $k_{\text{par}} < k_{\max}$  and zero transmission  $k_{\text{par}} > k_{\max}$ , then the image amplitude will vary with distance  $x$  parallel to the crystal surface as  $\left| \int_{-k_{\max}}^{k_{\max}} \exp[ik_{\text{par}}x] dk_{\text{par}} \right| = \left| 2 \sin(k_{\max}x) / (k_{\max}x) \right|$ , so that the resolution limit  $\Delta_{\min} = \pi/k_{\max} = 3a/4$ . This condition gives  $\Delta_{\min} = 0.34\lambda$  at 0.53 MHz, which is very close to the experimental and FDTD results.

These experimental and theoretical results demonstrate the conditions needed to achieve optimal focusing: (i) the equifrequency surfaces/contours should be spherical/circular, (ii) the equifrequency surfaces in the phononic crystal and in the medium outside should be matched, and (iii), for super resolution to be attained, the crystal should have a bound mode at a frequency close to the operational frequency, in order to enable amplification of evanescent waves from the source. The analysis of the maximum possible resolution that can be obtained with the 2D methanol-steel phononic crystal is relevant for designing new phononic crystal lenses in which the super resolution may be enhanced.

Our research on the development of new flat phononic crystal lenses has stimulated many other groups to investigate and further develop phononic crystal lenses using a variety of materials and approaches<sup>11-12, 15-21</sup>. Examples of new developments by other researchers include different 2D phononic crystal lenses that exploit negative refraction<sup>11, 12, 15-21</sup>, focusing studies with Lamb waves and surface acoustic waves<sup>22-30</sup>, and other types of flat lenses for acoustic waves (e.g., GRIN lenses<sup>26, 30-32</sup>). A related area is negative refraction and/or imaging with acoustic and elastic metamaterials<sup>33-43</sup>, where there has already been very

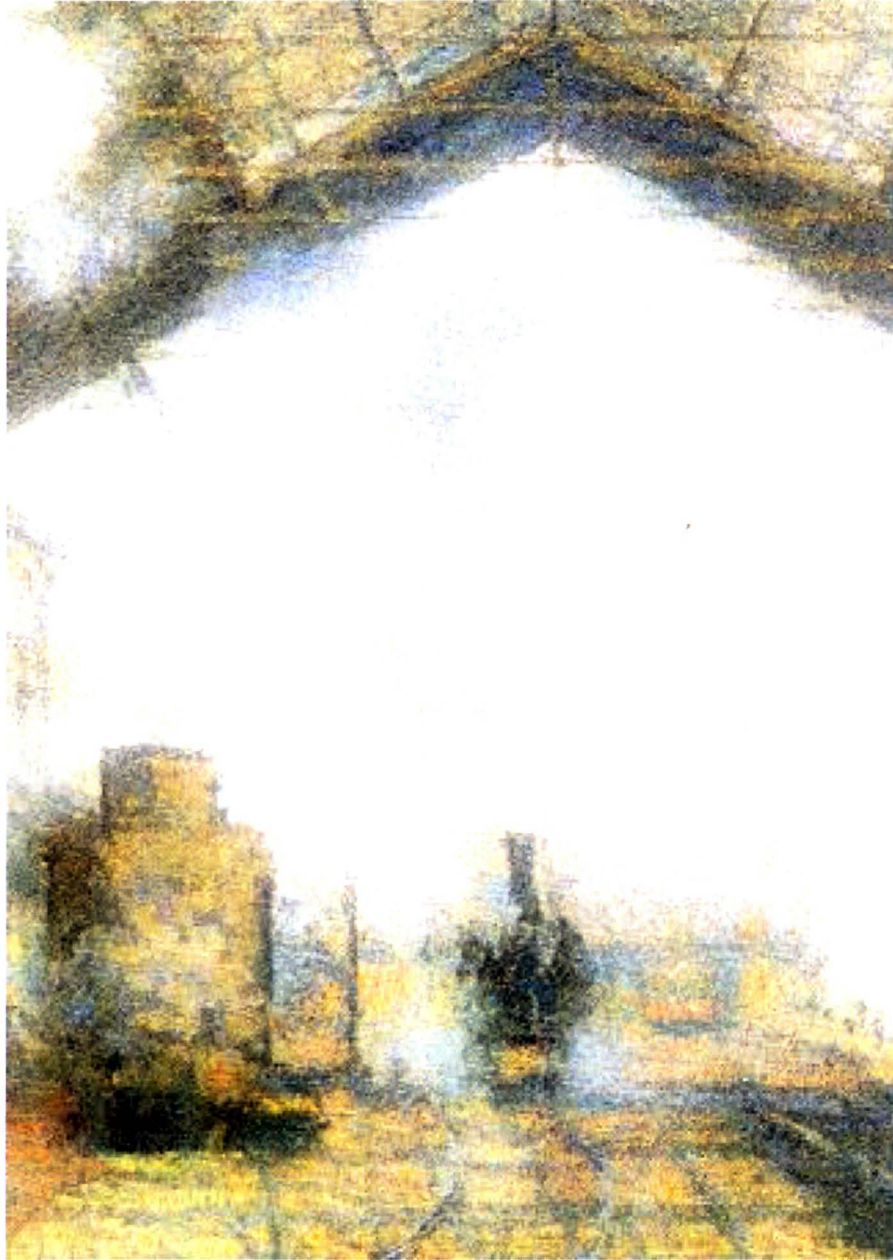
<sup>b</sup> Note that since the bound mode that is excited is a slab mode of the crystal, it is the bulk Brillouin zone boundary and not the surface Brillouin zone boundary that sets the resolution limit, allowing better resolution to be achieved for this triangular lattice than would be found for the surface modes that were considered by Luo et al. for photonic crystals.

significant progress and promise of increasing interest in the future. Potential applications that have been proposed include enhanced imaging for medical diagnoses, sonar and ultrasonic non-destructive evaluations, and even novel micromechanical actuators and sensors.

**Acknowledgements:** We wish to thank the following former students and colleagues for their contributions to the work over the past 15 years: Alexey Sukhovich, M.L. Cowan, Ping Sheng, C.T. Chan, P.A. Deymier, J.O. Vasseur, Y. Pennec, B. Merheb, J.F. Robillard, L. Jing, K. Mulidharan and A. Shelke. J.H.P. also gratefully acknowledges support from NSERC's Discovery Grant Program.

### References:

- <sup>1</sup> B. Taylor, H.J. Maris and C. Elbaum, *Phys. Rev. Lett.* **23**, 416 (1969).
- <sup>2</sup> J.P. Wolfe, *Imaging Phonons: Acoustic Wave Propagation in Solids* (Cambridge University Press, Cambridge, UK, 1998).
- <sup>3</sup> J. B. Pendry, *Phys. Rev. Lett.* **85**, 3966 (2000).
- <sup>4</sup> S. Yang, J.H. Page, Z. Liu, M.L. Cowan, C.T. Chan, P. Sheng, *Phys. Rev. Lett.* **93**, 024301 (2004)
- <sup>5</sup> A. Sukhovich, Li Jing and J.H. Page, *Phys. Rev. B*, **77**, 014301 (2008).
- <sup>6</sup> A. Sukhovich et al., *Phys. Rev. Lett.*, **102**, 154301 (2009).
- <sup>7</sup> A. Sukhovich and J.H. Page, "Phononic Crystals", in *2006 McGraw-Hill Yearbook of Science and Technology*, pp. 230-233 (2006).
- <sup>8</sup> A. Sukhovich et al., in *Phononic Crystals and Acoustic Metamaterials*, ed. by Pierre Deymier (Springer Solid State Science Series, 2013), chapter 4, pp. 95-158.
- <sup>9</sup> Suxia Yang, J. H. Page, Zhengyou Liu, M. L. Cowan, C.T. Chan and Ping Sheng, *Phys. Rev. Lett.* **88**, 104301 (2002).
- <sup>10</sup> Z. Liu, C.T. Chan, Ping Sheng, A.L. Goertzen and J.H. Page, *Phys. Rev. B*, **62**, 2446 (2000).
- <sup>11</sup> L. Feng et al, *Phys. Rev. B* **72**, 033108 (2005); *Phys. Rev. Lett.*, **96**, 014301 (2006).
- <sup>12</sup> M. Ke, Z. Liu, C. Qiu, W. Wang, J. Shi, W. Wen, and P. Sheng, *Phys. Rev. B* **72**, 064306 (2005).
- <sup>13</sup> M.-H. Lu et al., *Nat. Materials* **6**, 744 (2007).
- <sup>14</sup> J.-F. Robillard et al., *Phys. Rev. B*, **83**, 224301 (2011).
- <sup>15</sup> A.-C. Hladky-Hennion, et al., *AIP Advances*, **1**(4), 041405 (2011).
- <sup>16</sup> B. Morvan, et al., *Appl. Phys. Lett.* **96**, 101905 (2010).
- <sup>17</sup> C. Croenne et al., *Phys. Rev. B*, **83**, 054301 (2011).
- <sup>18</sup> E.D. Manga et al., *2011 IEEE Internat. Ultrasonics Symp.*, p 2491 (2012).
- <sup>19</sup> A.-C. Hladky-Hennion et al., *Appl. Phys. Lett.*, **102** 144103 (2013).
- <sup>20</sup> D. Bigoni et al., *Phys. Rev. B* **87**, 174303 (2013).
- <sup>21</sup> X. Zhou, M.B. Assouar and M. Oudich, *Appl. Phys. Lett.* **105**, 233506 (2014).
- <sup>22</sup> J. Pierre, O. Boyko, L. Belliard, J. Vasseur and B. Bonello, *Appl. Phys. Lett.* **97**, 121919 (2010).
- <sup>23</sup> I.A. Veres, T. Berer, O. Matsuda, P. Burgholzer, *J. Appl Phys.* **112**, 053504 (2012).
- <sup>24</sup> S. Bramhavar et al, *Phys. Rev. B* **83**, 014106 (2011).
- <sup>25</sup> M.A. Al-Lethawe, M. Addouche, A. Khelif, S. Guenneau, *New J. Phys.*, **14**, 123030 (2012).
- <sup>26</sup> Tsung-Tsong Wu and Chun-Wei Chen, *IEEE International Ultrasonics Symposium* (2012).
- <sup>27</sup> M. Dubois et al., *Appl. Phys. Lett.* **103**, 071915 (2013).
- <sup>28</sup> H. Jia, et al., *Appl. Phys. Lett.*, **103**, 103505 (2013).
- <sup>29</sup> M. Addouche, M.A. Al-Lethawe, A. Choujaa, and A. Khelif, *Appl. Phys. Lett.*, **105**, 023501 (2014).
- <sup>30</sup> J.F. Zhao, R. Marchal, B. Bonello, B. O. Boyko, *Appl. Phys. Lett.* **101**, 261905 (2012).
- <sup>31</sup> V. Romero-Garcia et al., *Appl. Phys. Lett.*, **103**, 264106 (2013).
- <sup>32</sup> V.M. Garcia-Chocano, J. Christensen, & J. Sánchez-Dehesa, *Phys. Rev. Lett.* **112**, 144301 (2014).
- <sup>33</sup> J. Li and C.T. Chan, *Phys. Rev. E*, **70**, 055602 (2004).
- <sup>34</sup> N. Fang, D. Xi, J. Xu, M. Ambati, W. Srituravanich, C. Sun and X. Zhang, *Nat. Mat.* **5**, 452 (2006).
- <sup>35</sup> Y. Ding, Z. Liu, C Qiu, and J. Shi, *Phys. Rev. Lett.* **99**, 093904 (2007).
- <sup>36</sup> M. Ambati, N. Fang, C. Sun, and X. Zhang, *Phys. Rev. B* **75**, 195447 (2007).
- <sup>37</sup> D. Torrent and J. Sanchez-Dehesa, *New Journal of Physics* **69**, 323 (2007).
- <sup>38</sup> J. Zhu, J. Christensen, et al., *Nature Phys.* **7**, 52 (2011).
- <sup>39</sup> F. Lemoult, M. Fink, and G. Lerosey, *Phys. Rev. Lett.*, **107**, 064301 (2011).
- <sup>40</sup> L. Fok and X. Zhang, *Phys. Rev. B* **83**, 214304 (2011).
- <sup>41</sup> J. Christensen and F.J.G. de Abajo, *Phys. Rev. Lett.*, **108**, 124301 (2012).
- <sup>42</sup> R. Zhu, X.N. Liu, G.K. Hu, C.T. Sun & G.L. Huang, *Nat. Commun.* **5**, 5510 (2014).
- <sup>43</sup> T. Brunet et al., *Nat. Materials*, published online 15 Dec. 2014 (DOI: 10.1038/NMAT4164).



*La gare Saint-Lazare,  
de Claude Monet*

The logo features a blue, multi-pointed star-like shape composed of overlapping, curved lines. To the right of this shape, the word "Phononics" is written in a large, bold, red sans-serif font. Below "Phononics", the year "2015" is displayed in a smaller, blue sans-serif font. Two horizontal red lines are positioned above and below the word "Phononics".

# Phononics

2015

3<sup>rd</sup> INTERNATIONAL CONFERENCE ON PHONONIC CRYSTALS/  
METAMATERIALS, PHONON TRANSPORT & PHONON COUPLING

